

Influence of ligands on the $fac \xrightleftharpoons{h\nu} mer$ isomerization in
[RuCl₃(NO)(P–P)] complexes, [P–P $\xrightleftharpoons{\Delta}$ R₂P(CH₂)_nPR₂ ($n = 1–3$)
and R₂P(CH₂)POR₂, PR₂–CH=CH–PR₂, R = Ph
and (C₆H₁₁)₂P–(CH₂)₂–P(C₆H₁₁)₂]

Gustavo Von Poelhsitz^{a,*}, Renata Cristina de Lima^a, Rose Maria Carlos^a,
Antonio Gilberto Ferreira^a, Alzir Azevedo Batista^{a,*}, Alexandre Suman de Araujo^b,
Javier Ellena^b, Eduardo Ernesto Castellano^b

^a Departamento de Química, Universidade Federal de São Carlos, C.P. 676, CEP 13565-905, São Carlos (SP), Brazil

^b Instituto de Física de São Carlos, Universidade de São Paulo, C.P. 369, CEP 13560-970, São Carlos (SP), Brazil

Received 1 November 2005; accepted 11 December 2005

Available online 18 January 2006

Dedicated to Professor Brian R. James on his 70th birthday.

Abstract

[RuCl₃(NO)(P–P)], [P–P = R₂P(CH₂)_nPR₂ ($n = 1–3$) and R₂P(CH₂)POR₂, PR₂–CH=CH–PR₂, R = Ph and (C₆H₁₁)₂P–(CH₂)₂–P(C₆H₁₁)₂] were obtained and characterized by ³¹P {¹H} NMR, IR spectroscopies and cyclic voltammetry. The structures of *fac*-[RuCl₃(NO)(P–P)], P–P = dppm (1), dppe (2), c-dppen (3) and dppp (4), *mer*-[RuCl₃(NO)(dcpe)] (6a) and *mer*-[RuCl₃(NO)(dppmO)] (7) have been determined by X-ray diffraction. Photochemical isomerization of *fac*- to *mer*-[RuCl₃(NO)(P–P)] was observed under white light in a CH₂Cl₂ solution and in solid state. The isomerization processes were followed by IR and ³¹P {¹H} spectra. The *mer*-[RuCl₃(¹⁵NO)(dppb)] isomer was used for the definition of the phosphorus atoms in the structure of the complex in solution. The electrochemical study shows that the oxidation/reduction processes observed in these complexes are dependent on both the isomer (*fac* or *mer*) and the solvent. In CH₂Cl₂, the NO⁺ reduction potentials are less negative for the *mer*-isomers than for the *fac* ones, while in CH₃CN solvent these potentials are, in general, very close for both isomers.

© 2005 Elsevier B.V. All rights reserved.

Keywords: Ruthenium; Diphosphines; Nitrosyl complexes; Photochemical isomerization; Electrochemistry; X-ray structures

1. Introduction

Nitric oxide is an interesting ligand for coordination chemistry, mainly because of its versatility in coordination to transition metals [1]. Also, NO is a very attractive and fascinating molecule and its biological functions were recognized in the 1980s [2,3]. Since then, nitrosyl complexes

have been seen as potential metalopharmaceutic drugs [4,5]. In this perspective, ruthenium appears as a good candidate due to the high affinity of nitric oxide for this metal [6,7]. In general the easiest accessible electroactive site in nitrosyl complexes is the NO⁺ ligand and a number of papers have described the NO labilization that can be promoted by photochemical or electrochemical reduction reactions [8–10]. As a strong π acid NO⁺ is able to promote the stabilization of some metallic centers and, depending on the electronic characteristics of the co-ligands in the metal coordination sphere, a one electron reduction process

* Corresponding authors. Tel.: +551633518285; fax: +551633518350.

E-mail addresses: gustavo@dq.ufscar.br (G. Von Poelhsitz), daab@power.ufscar.br (A.A. Batista).

involving the nitrosyl can be electrochemically reversible [10] or irreversible [11].

In the last years our research group has been interested in the nitrosyl ruthenium complexes containing diphosphine ligands, with the general formula $[\text{RuCl}_3(\text{NO})(\text{P}-\text{P})]$ [P–P = bis(diphenylphosphino)methane (dppm), 1,2-bis(diphenylphosphino)ethane (dppe), *cis*-1,2-bis(diphenylphosphino)ethylene (c-dppen), 1,3-bis(diphenylphosphino)propane (dppp) and 1,4-bis(diphenylphosphino)butane (dppb)] [12–15]. Thus several compounds with *fac* and/or *mer* geometries have been synthesized and fully characterized including X-ray crystallography analysis. These nitrosyl-compounds can be very useful as precursors to synthesize a variety of derivatives by substitution of the chlorides ligands as demonstrated by the reactions between *fac*- $[\text{RuCl}_3(\text{NO})(\text{P}-\text{P})]$, P–P = dppe or c-dppen, and 4,6-dimethyl-pyrimidine-2-thiolate ('SpymMe₂') to generate compounds with general formula $[\text{Ru}(\text{'SpymMe}_2\text{'}, -N, -S)(\text{'SpymMe}_2\text{'}, -S)(\text{NO})(\text{P}-\text{P})]^+$ [16]. Here we present a systematic route for the synthesis of the *mer*- $[\text{RuCl}_3(\text{NO})(\text{P}-\text{P})]$ isomers starting from the corresponding *fac*-isomers. Additionally, the electrochemical characterization of both *fac* and *mer* isomers is presented. A new member of this series with P–P = 1,2-bis(dicyclohexylphosphino)ethane (dcpe) was obtained. The X-ray structures of the *fac*- $[\text{RuCl}_3(\text{NO})(\text{dppm})]$ (**1**), *fac*- $[\text{RuCl}_3(\text{NO})(\text{dppe})]$ (**2**), *fac*- $[\text{RuCl}_3(\text{NO})(\text{c-dppen})]$ (**3**), *fac*- $[\text{RuCl}_3(\text{NO})(\text{dppp})]$ (**4**), *mer*- $[\text{RuCl}_3(\text{NO})(\text{dcpe})]$ (**6a**) and *mer*- $[\text{RuCl}_3(\text{NO})(\text{dppmO})]$ (**7**) complexes are reported here.

2. Experimental

2.1. Materials and methods

All the syntheses of the complexes were performed under argon. Solvents were purified by standard methods. All chemicals used were of reagent grade or comparable purity. The $\text{RuCl}_3 \cdot 3\text{H}_2\text{O}$ was purchased from Degussa or Aldrich and the diphosphine ligands were purchased from Aldrich or Strem. The $\text{Na}^{15}\text{NO}_2$ (min. 98%) was purchased from ISOTEC. The $\text{RuCl}_3\text{NO} \cdot 2\text{H}_2\text{O}$, *fac*- $[\text{RuCl}_3(\text{NO})(\text{P}-\text{P})]$, P–P = dppm (**1**), dppe (**2**), c-dppen (**3**) and dppp (**4**), *mer*- $[\text{RuCl}_3(\text{dppb})(\text{H}_2\text{O})]$, *fac* (**5**) and *mer* (**5a**)- $[\text{RuCl}_3(\text{NO})(\text{dppb})]$ were prepared according to the literature methods [12–14,17]. Yields are based on the metal.

2.2. Instrumentation

The infrared spectra were measured from powder samples diluted in CsI or in CH_2Cl_2 solutions using CaF_2 windows on an FTIR Bomem-Michelson 102 spectrometer in the 4000–200 cm^{-1} region for CsI samples and 4000–1000 cm^{-1} for solutions. UV–Vis spectra were recorded in a Cary 500 spectrophotometer. All the NMR experiments were recorded on a BRUKER equipment 9.4 T (400 MHz for hydrogen frequency). The ^{31}P $\{^1\text{H}\}$ and

^{15}N $\{^1\text{H}\}$ NMR spectra were recorded in CH_2Cl_2 using a capillary of D_2O to get the lock and H_3PO_4 (85%) and CH_3NO_2 as external references, respectively. Cyclic voltammetry (CV) experiments were carried out at room temperature in CH_2Cl_2 or CH_3CN containing 0.10 M $\text{Bu}_4\text{N}^+\text{ClO}_4$ (TBAP) (Fluka Purum) using a BAS-100B/W Bioanalytical Systems Instrument; the working and auxiliary electrodes were stationary Pt foils; a Luggin capillary probe was used and the reference electrode was Ag/AgCl. In these conditions the ferrocene is oxidized at 0.43 V (Fc^+/Fc) in CH_2Cl_2 or in CH_3CN . The microanalyses were performed by Microanalytical Laboratory of Universidade Federal de São Carlos, São Carlos (SP), using a FISIONS CHNS, mod. EA 1108 micro analyser.

2.3. Synthesis

2.3.1. *mer*- $[\text{RuCl}_3(\text{NO})(\text{P}-\text{P})]$, P–P = dppm (**1a**), dppe (**2a**), c-dppen (**3a**) and dppp (**4a**)

A CH_2Cl_2 (20 mL) solution/suspension of 50 mg (≈ 0.079 mmol) of the correspondent *fac*-complex was left under magnetic stirring for two weeks in an ordinary glass flask, not protected by light. Day by day the amount of solubilized complex increased as could be observed visually by the intensity of the color of the solution. The end of the reaction was confirmed by ^{31}P $\{^1\text{H}\}$ NMR spectroscopy and the volume of the solution was concentrated to ca. 1 mL and diethyl ether was added to give a yellow precipitate.

(**1a**) Yield: 42 mg (84%). IR (CsI, cm^{-1}): $\nu_{\text{Ru}-\text{Cl}}$ = 343; 286 w. UV–Vis (CH_2Cl_2) λ_{max} nm (log ϵ): 276 (4.17), 320 (3.73), 422 (2.63). Calc. for $\text{C}_{25}\text{H}_{22}\text{Cl}_3\text{P}_2\text{NORu}$: C, 48.29; H, 3.57; N, 2.25. Found: C, 48.38; H, 3.54; N, 2.30%.

(**2a**) Yield: 45 mg (90%). IR (CsI, cm^{-1}): $\nu_{\text{Ru}-\text{Cl}}$ = 345; 287 w. UV–Vis (CH_2Cl_2) λ_{max} nm (log ϵ): 276 (4.20), 324 (3.68), 420 (2.70). Calc. for $\text{C}_{26}\text{H}_{24}\text{Cl}_3\text{P}_2\text{NORu}$: C, 49.11; H, 3.80; N, 2.20. Found: C, 48.95; H, 3.59; N, 2.19%.

(**3a**) Yield: 40 mg (80%). IR (CsI, cm^{-1}): $\nu_{\text{Ru}-\text{Cl}}$ = 345; 288 w. UV–Vis (CH_2Cl_2) λ_{max} nm (log ϵ): 272 (4.17), 323 (3.61), 413 (2.69), 580 (2.07). Calc. for $\text{C}_{26}\text{H}_{22}\text{Cl}_3\text{P}_2\text{NORu}$: C, 49.27; H, 3.50; N, 2.21. Found: C, 49.67; H, 3.45; N, 2.29%.

(**4a**) Yield: 37 mg (74%). IR (CsI, cm^{-1}): $\nu_{\text{Ru}-\text{Cl}}$ = 337; 291 w. UV–Vis (CH_2Cl_2) λ_{max} nm (log ϵ): 245 (4.27), 272 (4.07) sh, 326 (3.40) sh, 425 (2.32). Calc. for $\text{C}_{27}\text{H}_{26}\text{Cl}_3\text{P}_2\text{NORu}$: C, 49.90; H, 4.03; N, 2.16. Found: C, 49.86; H, 4.14; N, 2.19%.

2.3.2. *fac*- $[\text{RuCl}_3(\text{NO})(\text{dcpe})]$ (**6**)

To a deoxygenated CH_3OH (25 mL) solution of the $\text{RuCl}_3\text{NO} \cdot 2\text{H}_2\text{O}$ precursor (50 mg, 0.18 mmol) was added 84 mg (0.20 mmol) of the dcpe ligand. After 2 h of magnetic stirring under Ar atmosphere, the yellow solution was filtered through celite. The resultant solution was concentrated until ca. 5 mL and diethyl ether was added to give a beige precipitate. Yield: 85 mg (70%). IR (CsI, cm^{-1}): $\nu_{\text{Ru}-\text{Cl}}$: 324; 279 w. UV–Vis (CH_2Cl_2) λ_{max} nm (log ϵ):

252 (4.19), 278 (4.01), 346 (3.37), 480 (2.24). Calc. for $C_{26}H_{48}Cl_3P_2NORu$: C, 47.31; H, 7.33; N, 2.12. Found: C, 47.61; H, 7.38; N, 2.29%.

2.3.3. *mer*-[RuCl₃(NO)(*dcpe*)] (**6a**)

Complex **6a** was obtained as described above for **1a–4a** starting with **6**. Yield: 40 mg, (80%). IR (CsI, cm⁻¹): ν_{Ru-Cl} : 338; 283 w. UV–Vis (CH₂Cl₂) λ_{max} nm (log ϵ): 269 (3.73), 320 (3.34), 421 (2.49). Calc. for $C_{26}H_{48}Cl_3P_2NORu$: C, 47.31; H, 7.33; N, 2.12. Found: C, 47.62; H, 7.29; N, 2.16%.

2.3.4. *mer*-[RuCl₃(NO)(*dppmO*)] (**7**)

The liquor mother of a synthesis of **1** was recovered and kept in a Becker cup at room temperature. After two days a great amount of red crystals was obtained. These crystals were identified as being **7**. IR (CsI, cm⁻¹): $\nu_{P=O}$ = 1122 s; ν_{Ru-Cl} : 342; 289 w. UV–Vis (CH₂Cl₂) λ_{max} nm (log ϵ): 274 (3.91), 432 (1.94). Calc. for $C_{25}H_{22}Cl_3P_2NO_2Ru$: C, 43.21; H, 3.35; N, 1.94. Found: C, 43.48; H, 3.33; N, 1.94%.

2.3.5. *mer*-[RuCl₃(¹⁵NO)(*dppb*)] (**8a**)

To a deoxygenated CH₂Cl₂ (15 mL) solution of *mer*-[RuCl₃(*dppb*)(H₂O)] (30 mg, 0.046 mmol) in a Schlenk flask was added Na¹⁵NO₂ (4.8 mg, 0.069 mmol) followed by 15 mL of 0.1 mol L⁻¹ HCl. The system was stopped and submitted to a strong magnetic stirring to mix up the two phases. After few seconds the color of the solution changed from red to green, but the reaction was maintained for 1 h, after which the two phases were separated. The organic phase containing the desired compound was concentrated to ca. 3 mL and diethyl ether was added precipitating a green solid. The product was collected by filtration, washed with water, and dried in vacuo. Yield: 24.5 mg, 80%. IR (CsI, cm⁻¹): ν_{Ru-Cl} = 340; 294 w. UV–Vis (CH₂Cl₂) λ_{max} nm (log ϵ): 251 (4.34), 276 (4.19), 334 (3.49), 436 (2.27). Calc. for $C_{28}H_{28}Cl_3P_2^{15}NORu$: C, 50.58; H, 4.24; N, 2.26. Found: C, 50.64; H, 4.24; N, 2.06%.

2.3.6. *fac*-[RuCl₃(¹⁵NO)(*dppb*)] (**8**)

The *fac*-[RuCl₃(¹⁵NO)(*dppb*)] complex was synthesized as previously reported for the synthesis of **5** [14]. Yield: 90%. IR (CsI, cm⁻¹): ν_{Ru-Cl} : 330; 287 w. UV–Vis (CH₂Cl₂) λ_{max} nm (log ϵ): 270 (4.27), 465 (1.95). Calc. for $C_{28}H_{28}Cl_3P_2^{15}NORu$: C, 50.58; H, 4.24; N, 2.26. Found: C, 50.66; H, 4.37; N, 2.08%.

2.4. X-ray crystallography

Compound **1** had previously been obtained in our research group [12] but co-crystallized with the *cis*-[RuCl₂(*dppm*)₂] complex. Compound **2** had also been obtained before but crystallized in a different space group [15]. The new structural results for these two compounds are reported here and discussed together with other members of the [RuCl₃(NO)(P–P)] series.

Crystals of the **1–4** complexes were grown by slow evaporation of dichloromethane/diethyl ether solutions.

For **6a**, crystals were grown by slow evaporation of methanol/diethyl ether solution. From the mother liquor of **1** were grown red crystals of **7**.

The crystals were mounted on an Enraf-Nonius Kappa-CCD diffractometer with graphite monochromated Mo K α (λ = 0.71073 Å) radiation. The final unit cell parameters were based on all reflections. Data collections were made using the COLLECT program [18]; integration and scaling of the reflections were performed with the HKL Denzo-Scalepack system of programs [19]. Absorption corrections were carried out using the “multi-scan” method [20] for **1**, **2**, **4** and **7**, integration [21] for **3** and gaussian [22] for **6a**. The structures were solved by direct methods with SHELXS-97 [23]. The model was refined by full-matrix least squares on F^2 by means of SHELXL-97 [24]. All hydrogen atoms were stereochemically positioned and refined with the riding model. Figs. 1–6 were prepared using ORTEP-3 for windows [25]. Hydrogen atoms of the aromatic rings and CH₂ were set isotropic with a thermal parameter 20% greater than the equivalent isotropic displacement parameter of the atom to which each one is bonded. The data collections and experimental details are summarized in Tables 1–3. The crystal structures of the complexes are shown in Figs. 1–6 and the selected bond distances and angles are given in Tables 4–7.

3. Results and discussion

3.1. Synthesis

The RuCl₃NO · 2H₂O precursor reacts with stoichiometric amount of the diphosphines *dppm*, *dppe*, *c-dppen*, *dppp* and *dcpe* to form the corresponding *fac* isomers with general formula [RuCl₃(NO)(P–P)]. However, with the *dppb* ligand, the reaction leads to the formation of a

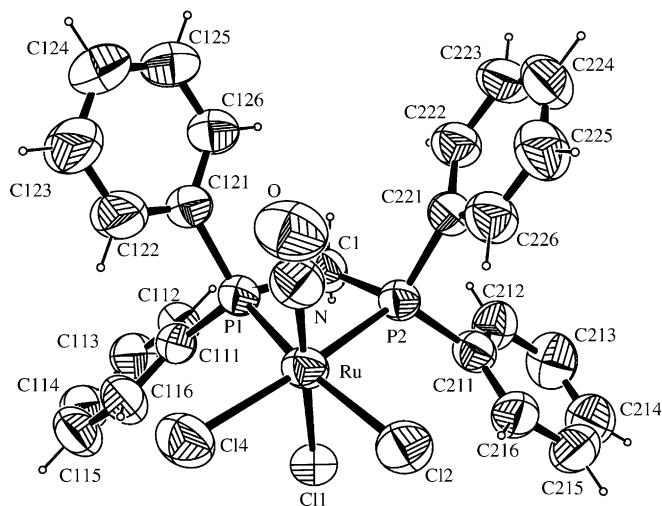


Fig. 1. ORTEP view of **1** showing the atoms labeling and the 50% probability ellipsoids.

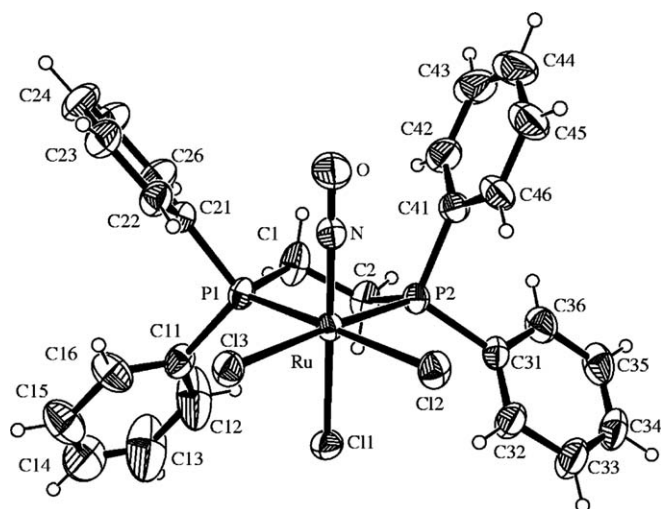


Fig. 2. ORTEP view of **2** showing the atoms labeling and the 30% probability ellipsoids.

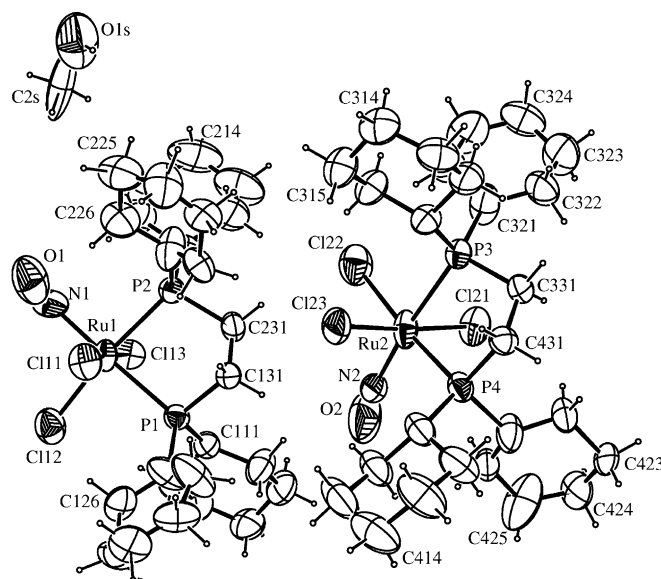


Fig. 5. ORTEP view of **6a** · CH₃OH showing the atoms labeling and the 50% probability ellipsoids.

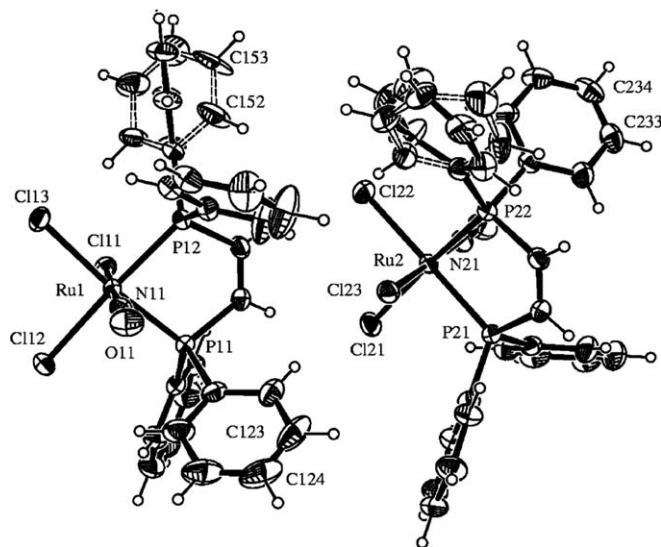


Fig. 3. ORTEP view of **3** showing the atoms labeling and the 50% probability ellipsoids.

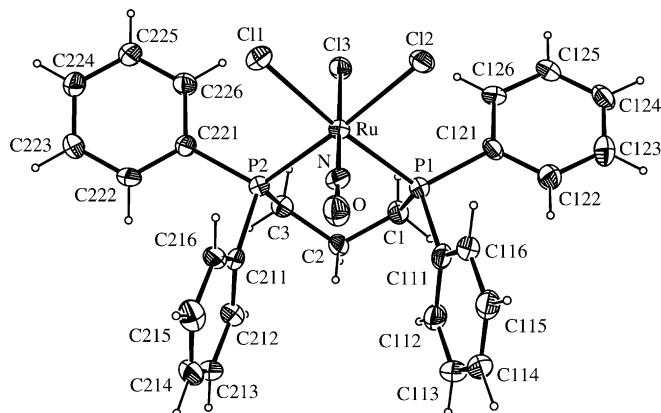


Fig. 4. ORTEP view of **4** showing the atoms labeling and the 50% probability ellipsoids.

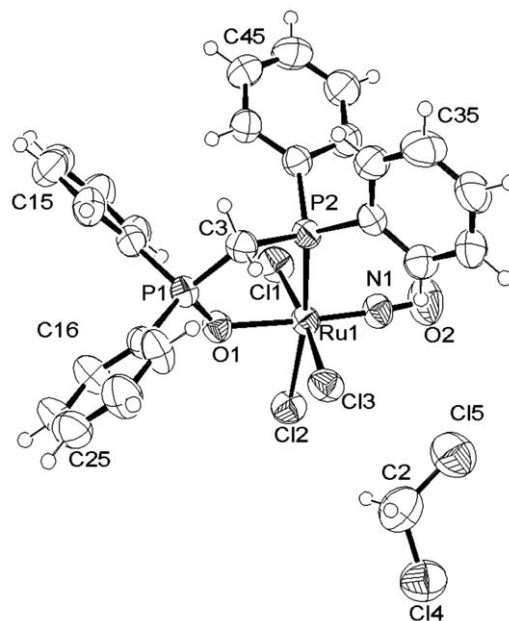


Fig. 6. ORTEP view of **7** · CH₂Cl₂ showing the atoms labeling and the 50% probability ellipsoids.

mixture of complexes detected by ³¹P {¹H} NMR spectroscopy. Using the aquo, *mer*-[RuCl₃(dppb)(H₂O)], previously obtained in our laboratory [17], and bubbling NO gas, it was possible to obtain **5a** with a high level of purity, as was shown by microanalysis data and a ³¹P {¹H} spectrum. The corresponding *fac* isomer **5** was isolated in quantitative yield by heating **5a** in methanol for 2 h. The *mer*-[RuCl₃(dppb)(H₂O)] was reacted with ¹⁵NO (generated from the Na¹⁵NO₂ and HCl 0.1 mol L⁻¹) in a biphasic reaction, generating **8a**. Following the same procedure described above, complex **8** was also isolated.

Table 1
Crystallographic data and refinement details for **1**, **2** and **4**

	1	2	4
Empirical formula	C ₂₅ H ₂₂ Cl ₃ NOP ₂ Ru	C ₂₆ H ₂₄ Cl ₃ NOP ₂ Ru	C ₂₇ H ₂₆ Cl ₃ NOP ₂ Ru
Formula weight	621.80	635.82	649.85
Temperature (K)	120(2)	293(2)	120(2)
Crystal system	monoclinic	orthorhombic	monoclinic
Space group	<i>C</i> ₂ / <i>c</i>	<i>Pbca</i>	<i>P</i> ₂ / <i>c</i>
<i>Unit cell dimensions</i>			
<i>a</i> (Å)	26.160(2)	16.1840(3)	16.4595(9)
<i>b</i> (Å)	15.433(1)	15.1020(2)	10.8249(5)
<i>c</i> (Å)	17.514(1)	22.5020(4)	16.4840(7)
β (°)	127.876(4)		115.259(2)
Volume (Å ³)	5581.3(7)	5499.73(16)	2656.2(2)
<i>Z</i>	8	8	4
Density (calculated) (g cm ⁻³)	1.480	1.536	1.625
Absorption coefficient (mm ⁻¹)	0.981	0.998	1.035
<i>F</i> (000)	2496	2560	1312
Crystal size (mm ³)	0.22 × 0.18 × 0.10	0.15 × 0.70 × 0.45	0.08 × 0.02 × 0.01
θ Range for data collection (°)	3.74–25.00	1.81–27.5	2.73–25.00
Limiting indices	–31 ≤ <i>h</i> ≤ 31 –17 ≤ <i>k</i> ≤ 18 –20 ≤ <i>l</i> ≤ 20	–21 ≤ <i>h</i> ≤ 21 –19 ≤ <i>k</i> ≤ 19 –29 ≤ <i>k</i> ≤ 28	–19 ≤ <i>h</i> ≤ 19 –12 ≤ <i>k</i> ≤ 12 –19 ≤ <i>l</i> ≤ 19
Reflections collected	8708	55055	14318
Independent reflections (<i>R</i> _{int})	4891 (0.0321)	6288 (0.0606)	4675 (0.1089)
Data/restraints/parameters	4891/0/298	6288/0/307	4675/0/317
Goodness-of-fit on <i>F</i> ²	1.047	1.180	1.091
Final <i>R</i> indices [<i>I</i> > 2σ(<i>I</i>)]	<i>R</i> ₁ = 0.0485, <i>wR</i> ₂ = 0.1327	<i>R</i> ₁ = 0.0423, <i>wR</i> ₂ = 0.1134	<i>R</i> ₁ = 0.0521, <i>wR</i> ₂ = 0.1135
<i>R</i> indices (all data)	<i>R</i> ₁ = 0.0646, <i>wR</i> ₂ = 0.1447	<i>R</i> ₁ = 0.0687, <i>wR</i> ₂ = 0.1414	<i>R</i> ₁ = 0.0743, <i>wR</i> ₂ = 0.1221
Peak and hole/e Å ⁻³	0.568 and –0.814	0.999 and –1.417	0.979 and –1.126

Table 2
Crystallographic data and refinement details for **3**

	Super-cell	Sub-cell
Empirical formula		C ₂₆ H ₂₂ Cl ₃ NOP ₂ Ru
Formula weight		633.81
Temperature (K)		293
Crystal system		triclinic
Space group		<i>P</i> ₁ ₂
<i>a</i> (Å)	16.3710(6)	16.3710(6)
<i>b</i> (Å)	18.1210(5)	11.3549(5)
<i>c</i> (Å)	18.7200(5)	14.5076(5)
α (°)	103.908(2)	88.081(2)
β (°)	97.384(2)	86.673(2)
γ (°)	92.283(2)	82.084(2)
Volume (Å ³)	5331.5(3)	2665.8(2)
<i>Z</i>	8	4
Density (calculated) (g cm ⁻³)		1.579
<i>F</i> (000)	2544	1272
Crystal size		0.285 × 0.059 × 0.022
Absorption coefficient (mm ⁻¹)		1.029
θ Range for data collection (°)	1.81–27.51	1.81–25
Limiting indices	0 ≤ <i>h</i> ≤ 21 –23 ≤ <i>k</i> ≤ 23 –24 ≤ <i>l</i> ≤ 24	0 ≤ <i>h</i> ≤ 19 –13 ≤ <i>k</i> ≤ 13 –17 ≤ <i>l</i> ≤ 17
Reflections collected	24317	9407
Independent reflections (<i>R</i> _{int})	24317 (0.000)	9407 (0.0630)
Data/parameters	24317/1225	9407/705
Goodness-of-fit on <i>F</i> ²	1.199	1.262
Final <i>R</i> indices [<i>I</i> > 2σ(<i>I</i>)]	<i>R</i> ₁ = 0.0682, <i>wR</i> ₂ = 0.1588	<i>R</i> ₁ = 0.0423, <i>wR</i> ₂ = 0.1184
<i>R</i> indices (all data)	<i>R</i> ₁ = 0.1432, <i>wR</i> ₂ = 0.2284	<i>R</i> ₁ = 0.0627, <i>wR</i> ₂ = 0.1582
Peak and hole (e Å ⁻³)	0.822 and –1.655	0.708 and –1.385

Table 3
Crystallographic data and refinement details for **6a** and **7**

	6a · CH ₃ OH	7 · CH ₂ Cl ₂
Empirical formula	C ₂₆ H ₄₈ Cl ₃ NOP ₂ Ru	C ₂₅ H ₂₂ Cl ₃ NO ₂ P ₂ Ru
Formula weight	728.4	722.72
Temperature (K)	293(2)	293(2)
Crystal system	triclinic	monoclinic
Space group	\bar{P}	$P2_1/n$
<i>Unit cell dimensions</i>		
<i>a</i> (Å)	12.2066(3)	10.4131(2)
<i>b</i> (Å)	15.5411(3)	16.0571(5)
<i>c</i> (Å)	17.5250(4)	17.6626(4)
α (°)	89.9580(10)	
β (°)	79.6110(10)	90.6230(10)
γ (°)	74.1000(10)	
Volume (Å ³)	3140.79(12)	2953.09(13)
<i>Z</i>	2	4
Density (calculated) (g cm ⁻³)	1.392	1.626
Absorption coefficient (mm ⁻¹)	0.876	1.117
<i>F</i> (000)	1365	1448
Crystal size	0.45 × 0.34 × 0.07	0.14 × 0.11 × 0.10
θ Range for data collection (°)	3.17–25.00	2.28–25.00
Limiting indices	–14 ≤ <i>h</i> ≤ 14 –17 ≤ <i>k</i> ≤ 18 –20 ≤ <i>l</i> ≤ 20	–12 ≤ <i>h</i> ≤ 12 18 ≤ <i>k</i> ≤ 19 –19 ≤ <i>l</i> ≤ 21
Reflections collected	20685	17134
Independent reflections (<i>R</i> _{int})	11048 (0.0382)	5184 (0.0462)
Data/restraints/parameters	11048/1/767	5184/0/335
Goodness-of-fit on <i>F</i> ²	1.042	1.180
Final <i>R</i> indices [<i>I</i> > 2σ(<i>I</i>)]	<i>R</i> ₁ = 0.0532, <i>wR</i> ₂ = 0.1345	<i>R</i> ₁ = 0.0618, <i>wR</i> ₂ = 0.1776
<i>R</i> indices (all data)	<i>R</i> ₁ = 0.0697, <i>wR</i> ₂ = 0.1449	<i>R</i> ₁ = 0.0698, <i>wR</i> ₂ = 0.1816
Peak and hole (e Å ⁻³)	0.798 and –1.171	0.913 and –0.653

Table 4
Selected bond distances (Å) for **1**, **2** and **4**

1		2		4	
Ru–N	1.787(6)	Ru–N	1.750(3)	Ru–N	1.734(5)
Ru–P(1)	2.3488(12)	Ru–P(1)	2.3637(9)	Ru–P(1)	2.3686(13)
Ru–P(2)	2.3582(11)	Ru–P(2)	2.3492(9)	Ru–P(2)	2.3971(13)
O–N	1.029(6)	O–N	1.128(5)	O–N	1.152(5)
Ru–Cl(1)	2.3584(12)	Ru–Cl(1)	2.350(1)	Ru–Cl(1)	2.4180(13)
Ru–Cl(4)	2.4231(14)	Ru–Cl(3)	2.429(1)	Ru–Cl(3)	2.3679(13)
Ru–Cl(2)	2.4288(13)	Ru–Cl(2)	2.4356(9)	Ru–Cl(2)	2.4068(13)

Under white light after a two weeks period the *fac*-[RuCl₃(NO)(P–P)] complexes, dissolved in CH₂Cl₂, isomerized to the *mer* species (Scheme 1).

Complex **7** was obtained from the liquor mother of **1**, but it was also obtained as a by-product during the *fac* to *mer* photoisomerization of **1**, as judged by a ³¹P {¹H} NMR spectrum. This result suggests that the oxidation of the phosphorus in complex **1** had occurred during the isomerization process, and it is worth pointing out that this oxidation process was detected only for this complex. The explanation for this may be the fact that the four member chelate of the dppm complex is very strained, generating a temporary “dangling” ligand and in the presence of oxygen the non coordinated phosphorus atom is quickly oxidized. The dppmO ligand formed is a five member chelate and its coordination to the metal via P–O is favorable, allowing the formation of **7**

(Scheme 2). When the isomerization of **1** is conducted under totally deoxygenated atmosphere (under pure Ar) the sole product formed is **1a**.

There are a number of reports showing nitrosyl complexes that are photoactive as NO⁰ donors [4,26–28] but, however, this is not the case for the complexes studied in this work. Irradiations with white light do not produce any change that could be attributed to NO⁰ dissociation. As will be shown by IR and ³¹P {¹H} NMR spectroscopies, the photolysis of *fac* leads to formation of the *mer* isomers.

3.2. Characterization

3.2.1. Infrared spectra

There are in the literature reports on solid state effects which cause split in the NO stretching band [29,30]. To

Table 5
Selected bond angles for (°) **1**, **2** and **4**

1		2		4	
N–Ru–P(1)	92.55(14)	N–Ru–P(1)	91.39(11)	N–Ru–P(1)	93.33(14)
N–Ru–P(2)	93.27(14)	N–Ru–P(2)	92.62(10)	N–Ru–P(2)	94.44(15)
P(1)–Ru–P(2)	71.26(4)	P(1)–Ru–P(2)	85.76(3)	P(1)–Ru–P(2)	93.22(5)
N–Ru–Cl(1)	175.93(14)	N–Ru–Cl(1)	176.94(11)	N–Ru–Cl(1)	90.13(14)
P(1)–Ru–Cl(1)	83.74(4)	P(1)–Ru–Cl(1)	86.08(4)	P(1)–Ru–Cl(1)	174.83(5)
P(2)–Ru–Cl(1)	83.96(4)	N–Ru–Cl(3)	92.07(10)	P(2)–Ru–Cl(1)	90.34(5)
N–Ru–Cl(4)	91.13(14)	P(1)–Ru–Cl(3)	92.16(3)	N–Ru–Cl(3)	179.05(14)
P(1)–Ru–Cl(4)	99.59(5)	P(2)–Ru–Cl(1)	83.96(4)	P(1)–Ru–Cl(3)	86.27(5)
O–N–Ru	178.7(6)	O–N–Ru	178.6(4)	O–N–Ru	176.9(4)
P(2)–Ru–Cl(4)	170.00(5)	P(2)–Ru–Cl(3)	174.91(4)	P(2)–Ru–Cl(3)	84.73(5)
Cl(1)–Ru–Cl(4)	91.15(5)	Cl(1)–Ru–Cl(3)	89.74(4)	Cl(1)–Ru–Cl(3)	90.33(5)
N–Ru–Cl(2)	92.09(15)	N–Ru–Cl(2)	91.91(11)	N–Ru–Cl(2)	90.76(14)
P(1)–Ru–Cl(2)	168.43(5)	P(1)–Ru–Cl(2)	175.32(4)	P(1)–Ru–Cl(2)	88.07(5)
P(2)–Ru–Cl(2)	97.90(5)	P(2)–Ru–Cl(2)	90.77(4)	P(2)–Ru–Cl(2)	174.56(5)
Cl(1)–Ru–Cl(2)	91.24(5)	Cl(1)–Ru–Cl(2)	90.52(4)	Cl(1)–Ru–Cl(2)	88.05(5)
Cl(4)–Ru–Cl(2)	90.90(5)	Cl(3)–Ru–Cl(2)	91.04(4)	Cl(3)–Ru–Cl(2)	90.08(5)

Table 6
Selected bond distances (Å) and angles (°) for **3**

Ru(1)–N(11)	1.738(4)	Ru(2)–N(21)	1.786(5)
Ru(1)–P(12)	2.3438(12)	Ru(2)–P(21)	2.3476(12)
Ru(1)–P(11)	2.3480(12)	Ru(2)–P(22)	2.3496(13)
Ru(1)–Cl(11)	2.3499(13)	Ru(2)–Cl(23)	2.3514(13)
Ru(1)–Cl(13)	2.4268(12)	Ru(2)–Cl(21)	2.4185(14)
Ru(1)–Cl(12)	2.4534(13)	Ru(2)–Cl(22)	2.4280(13)
O(11)–N(11)	1.143(6)	O(21)–N(21)	1.051(6)
N(11)–Ru(1)–P(12)	92.61(14)	N(21)–Ru(2)–P(21)	93.82(14)
N(11)–Ru(1)–P(11)	93.37(14)	N(21)–Ru(2)–P(22)	91.94(14)
P(12)–Ru(1)–P(11)	84.26(4)	P(21)–Ru(2)–P(22)	84.45(4)
N(11)–Ru(1)–Cl(11)	176.67(14)	N(21)–Ru(2)–Cl(23)	175.14(14)
P(12)–Ru(1)–Cl(11)	87.49(5)	P(21)–Ru(2)–Cl(23)	84.94(4)
P(11)–Ru(1)–Cl(11)	83.33(5)	P(22)–Ru(2)–Cl(23)	83.27(5)
N(11)–Ru(1)–Cl(13)	93.14(14)	N(21)–Ru(2)–Cl(21)	95.13(15)
P(12)–Ru(1)–Cl(13)	90.53(4)	P(21)–Ru(2)–Cl(21)	90.68(5)
P(11)–Ru(1)–Cl(13)	171.84(5)	P(22)–Ru(2)–Cl(21)	171.67(5)
Cl(11)–Ru(1)–Cl(13)	90.18(5)	Cl(23)–Ru(2)–Cl(21)	89.59(5)
N(11)–Ru(1)–Cl(12)	89.33(14)	N(21)–Ru(2)–Cl(22)	88.15(15)
P(12)–Ru(1)–Cl(12)	175.73(5)	P(21)–Ru(2)–Cl(22)	177.80(5)
P(11)–Ru(1)–Cl(12)	91.83(5)	P(22)–Ru(2)–Cl(22)	94.52(5)
Cl(11)–Ru(1)–Cl(12)	90.36(5)	Cl(23)–Ru(2)–Cl(22)	93.02(5)
Cl(13)–Ru(1)–Cl(12)	93.16(5)	Cl(21)–Ru(2)–Cl(22)	90.12(5)
O(11)–N(11)–Ru(1)	179.0(4)	O(21)–N(21)–Ru(2)	175.7(5)

avoid this effect, in this work the IR spectra were obtained in CH₂Cl₂ solutions and CsI pellets (see Table 8).

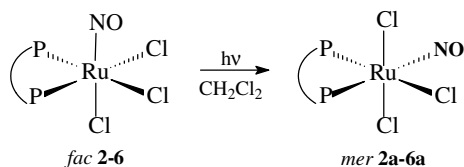
The IR spectra of the complexes are dominated by the strong NO stretching band (ν_{NO}) in the range of 1818–1884 cm⁻¹ [31] depending on the isomer and the diphosphine. Important bands are also those involving the Ru center and the chloride ligands in the low energy region [32]. Comparing the *fac* and the *mer* isomers there is a marked difference in the Ru–Cl stretching vibration modes; the *fac*-ones are characterized by these bands occurring in the range of 327–330 cm⁻¹ while in the *mer* isomers the $\nu_{\text{Ru–Cl}}$ bands are in the range of 337–345 cm⁻¹. The other bands in the IR spectra are due to the vibrational modes of the diphosphine ligands, being only slightly affected by the coordination to the metal center [33].

Comparing the ν_{NO} bands obtained in CsI pellets and CH₂Cl₂ solutions for the same complex they are seen to be generally different. In going from pellets to solutions the ν_{NO} for the *fac* isomers shift to lower frequencies while the *mer* isomers show opposite behavior. However the differences are not constant, being dependent on the compound.

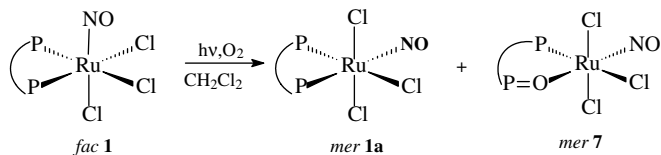
Three of the *mer*-isomers (**1**, **2** and **3**) show ν_{NO} values smaller than those in the corresponding *fac*; however, the opposite occurs for the pair **5/5a**, and for the compounds **4/4a** and **6/6a** the ν_{NO} is independent of the isomer. Considering only electronic aspects, the ν_{NO} should shift to lower frequencies in the *mer* than in the *fac* isomers because the ruthenium center is expected to be electron richer in the former (two chlorides in *trans* cause a strong competitive effect). However this characteristic is not constant in this

Table 7
Selected bond distances (Å) and angles for (°) **6a** and **7**

6a		7	
Ru(1)–N(1)	1.971(6)	Ru(2)–N(2)	1.940(5)
Ru(1)–P(2)	2.4015(12)	Ru(2)–P(4)	2.3922(14)
Ru(1)–P(1)	2.4563(12)	Ru(2)–P(3)	2.4529(13)
Ru(1)–Cl(11)	2.3748(14)	Ru(2)–Cl(23)	2.3718(14)
Ru(1)–Cl(13)	2.3723(12)	Ru(2)–Cl(21)	2.3884(14)
Ru(1)–Cl(12)	2.3759(16)	Ru(2)–Cl(22)	2.3726(18)
O(11)–N(11)	0.789(8)	O(21)–N(21)	0.866(7)
N(1)–Ru(1)–P(2)	93.1(2)	N(2)–Ru(2)–P(3)	171.95(16)
N(1)–Ru(1)–P(1)	174.29(18)	N(2)–Ru(2)–P(4)	95.14(19)
P(2)–Ru(1)–P(1)	84.26(4)	P(3)–Ru(2)–P(4)	83.86(4)
N(1)–Ru(1)–Cl(11)	90.62(18)	N(2)–Ru(2)–Cl(23)	95.70(17)
P(2)–Ru(1)–Cl(11)	92.88(5)	P(3)–Ru(2)–Cl(23)	92.25(5)
P(1)–Ru(1)–Cl(11)	84.46(5)	P(4)–Ru(2)–Cl(23)	88.51(5)
N(1)–Ru(1)–Cl(13)	93.94(18)	N(2)–Ru(2)–Cl(21)	89.00(17)
P(2)–Ru(1)–Cl(13)	86.94(4)	P(3)–Ru(2)–Cl(21)	83.05(5)
Ru–N	1.713(6)	Ru–O(1)	2.059(5)
Ru–P(2)	2.3597(19)	O–N	1.147(9)
Ru–Cl(1)	2.367(2)	Ru–Cl(3)	2.3665(18)
Ru–Cl(2)	2.404(2)	Ru–Cl(1)	2.526(5)
O(1)–P(1)	1.526(5)	N–Ru–O(1)	176.1(3)
N–Ru–O(1)	176.1(3)	N–Ru–P(2)	92.3(2)
N–Ru–P(2)	92.3(2)	O(1)–Ru–P(2)	83.94(14)
O(1)–Ru–P(2)	83.94(14)	N–Ru–Cl(1)	91.4(2)
N–Ru–Cl(1)	91.4(2)	O(1)–Ru–Cl(1)	88.13(15)
O(1)–Ru–Cl(1)	88.13(15)	P(2)–Ru–Cl(1)	93.00(7)
P(2)–Ru–Cl(1)	93.00(7)	N–Ru–Cl(3)	94.7(2)
N–Ru–Cl(3)	94.7(2)	O(1)–Ru–Cl(3)	85.98(14)
O(1)–Ru–Cl(3)	85.98(14)		



Scheme 1. The *fac* to *mer* isomerization process for the *fac*-[RuCl₃(NO)-(P–P)] complexes.



Scheme 2. The *fac* to *mer* isomerization process for the *fac*-[RuCl₃(NO)-(dppm)] complex.

series probably because for some compounds, steric factors may affect the properties of the coordinated NO. This is apparent when considering that the compounds with opposite behavior contain the more steric demanding diphosphines (dppp, dppb and dcpe), as can be seen by their

Table 8
IR (ν_{NO}) bands (cm^{-1}) and ^{31}P { ^1H } NMR data for the [RuCl₃(NO)(P–P)] complexes

P–P	ν_{NO}		δ ^{31}P (ppm)				$^2J_{\text{P–P}}$ (Hz)	
	CH_2Cl_2		CsI		<i>fac</i>	<i>mer</i>		
	<i>fac</i>	<i>mer</i>	<i>fac</i>	<i>mer</i>	P_{A}	P_{B}		
dppm	1872	1838	1876	1834	–15.3	–9.9	–32.1	68.2
dppe	1866	1858	1874	1839	46.9	54.6	35.6	23.6
c-dppen	1883/1874	1851	1884/1876	1828	55.3	63.8	46.8	12.8
dppp	1870	1870	1875	1843	15.6	10.4	0.78	49.8
dppb	1855	1880	1868	1868	22.8	13.6	10.1	37.5
dcpe	1850	1851	1838	1821	62.9	67.1	44.0	18.2
dppmO		1878		1858		67.9 (P ^{III})	40.6 (P ^V)	23.0
$^{15}\text{NOdppb}$	1818	1843	1831	1831	22.5	14.2	10.7 ^a	36.9

^a $^2J_{\text{P–N}} = 72.2$ Hz.

cone angles which are bigger than in dppm, dppe and c-dppen [34].

The sequence of IR spectra obtained during the solid state *fac* to *mer* isomerization **1** in CsI pellets under irradiation with white lamp is shown in Fig. 7.

All the complexes with *fac* geometry presented the same behavior of solid state isomerization, but when the *mer* isomers are irradiated following the same procedure described above, there are no changes in the IR spectra.

In complexes **8** and **8a** the NO stretching band is shifted 37 cm^{-1} towards lower energy when compared with the ^{14}NO analogous, **5** and **5a**; for both isomers $\nu_{\text{NO}}^{14}/\nu_{\text{NO}}^{15} = 1.020$, a value very close to the theoretical one calculated from the Hooke law (1.018) [35]. The $\nu_{\text{Ru–N}}$ and the $\delta_{\text{Ru–N–O}}$ bands appear at 592 and 527 cm^{-1} for **8** and 577 and 515 cm^{-1} for **8a** [32]. Similar differences are found for the complex *trans*-[RuCl(NO)(das)₂]Cl₂ when compared with the analogous ^{15}NO [36].

3.2.2. ^{31}P { ^1H } and ^{15}N { ^1H } NMR spectra

The ^{31}P { ^1H } NMR spectra of the *fac*-[RuCl₃(NO)(P–P)] series are characterized by a singlet, indicating the magnetic equivalence of the phosphorus atoms [12]. For the *mer* compounds a pair of doublets are observed in the spec-

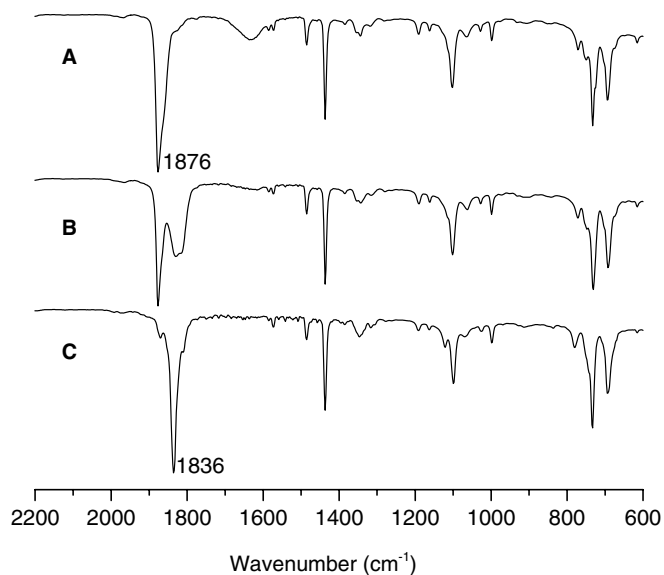


Fig. 7. Sequence of IR spectra (CsI) showing the *fac* (ν_{NO} at 1876) to *mer* (ν_{NO} at 1836) isomerization of **1**. Irradiation A–B: 20 min; A–C (90 min) with a white lamp.

tra, showing that the phosphorus are *trans* to different atoms, NO and Cl.

All the chemical shifts observed are in agreement with the ring size effect in which the order of shielding is four > six > seven > five member ring [37]. In spite of the fact that compounds **2/2a**, **3/3a** and **6/6a** have five member rings, compounds **6/6a** are more deshielded, possibly as a consequence of the steric effect caused by the cyclohexyl rings, which can distort more effectively the internal ring angle of the P–Ru–P bite. For compounds **3/3a** the main effect is the electron-withdraw produced by the π orbitals from the carbon-carbon double bond. Table 8 shows the ^{31}P { ^1H } NMR data for all the complexes and Fig. 10 shows the NMR ^{31}P { ^1H } data correlations (chemical shifts versus coupling constant) for the *mer* isomers.

The phosphorus *trans* to the NO are more distant from the metal center, as has been shown by X-ray analysis [13,14]. Thus their chemical shifts become closer to the ones

of the free phosphines, that is, the phosphorous atoms are in these cases more shielded. For this reason the higher field doublets can be attributed to the phosphorus *trans* to the NO group. To verify this proposition the *mer*-[RuCl₃(¹⁵NO)(dppb)] (**8a**) was synthesized. The ^{31}P { ^1H } NMR spectrum shown in Fig. 8(A) presents two sets of signals, a doublet at lower field and a double doublet (dd) at higher field, indicating an AMX spin system. The dd pattern indicates that P_B is coupled to P_A, with $^2J_{\text{P-P}} = 36.9$ Hz, and with the ¹⁵N of the ¹⁵NO group with $^2J_{\text{P-N}} = 72.2$ Hz, which is a typical value for *trans* coupling P–¹⁵N [38]. This result confirms the previous attribution to the phosphorus chemical shifts in this class of compounds [13,14]. In the ¹⁵N NMR spectrum of **8a**, shown in Fig. 8(B), an AX double doublet (dd) is observed at –30.0 ppm with $^2J_{\text{P-N}} = 72.2$ Hz (*trans*) and $^2J_{\text{P-N}} = 3.2$ Hz (*cis*). The corresponding spectra for the *fac* isomer **8**, given in Fig. 9, show that the spectrum lines become simpler because the phosphorus are magnetically equivalent in this case. In the ^{31}P { ^1H } NMR of **8**, a doublet appeared at 23.0 ppm with $^2J_{\text{P-N}} = 3.2$ Hz (*cis*). In the ¹⁵N NMR spectra of **8**, an AB triplet system t(AB) is observed at –54.0 ppm with $^2J_{\text{P-N}} = 3.2$ Hz (*cis*); this pattern arises due to the coupling between ¹⁵N with two almost equivalent phosphorus. The slightly lower ¹⁵N chemical shift in **8** than in **8a** indicates that in **8** there is a more linear nitrosyl group and that in both complexes the chemical shifts are typical of the ¹⁵NO⁺ ligand [39].

Fig. 10 is a graph correlating the NMR data for coupling constants (Table 8) versus chemical shifts of the P *trans* NO, suggesting a direct correlation between these two phenomena in this series of *mer*-[RuCl₃(NO)(P–P)] complexes.

3.3. Isomerization of *mer* to *fac*-isomers

Previous reports [12,13] have shown that **4a** and **5a** in solution of CH₂Cl₂ undergo an isomerization process to form the *fac* isomer; for **4a** the conversion is total while for **5a** it is partial. The new *mer* complexes obtained in this

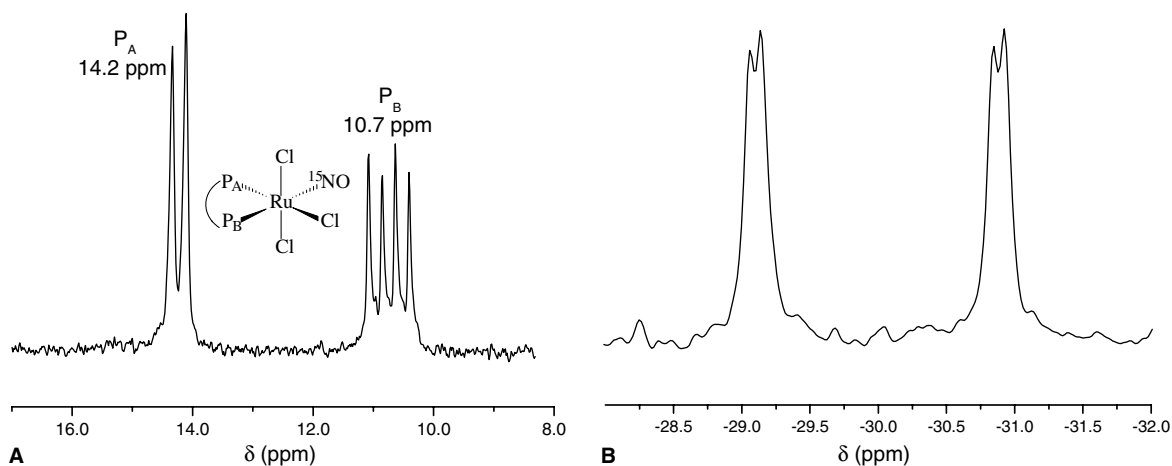


Fig. 8. NMR spectra of **8a** in CH₂Cl₂. (A) ^{31}P { ^1H }. (B) ^{15}N { ^1H }.

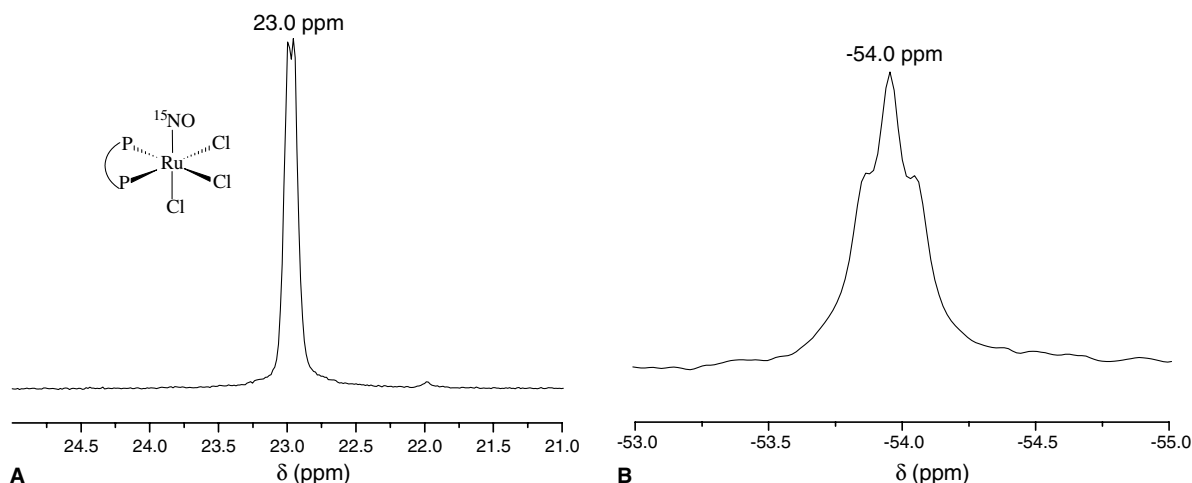


Fig. 9. NMR spectra of **8** in CH_2Cl_2 . (A) ^{31}P $\{^1\text{H}\}$. (B) ^{15}N $\{^1\text{H}\}$.

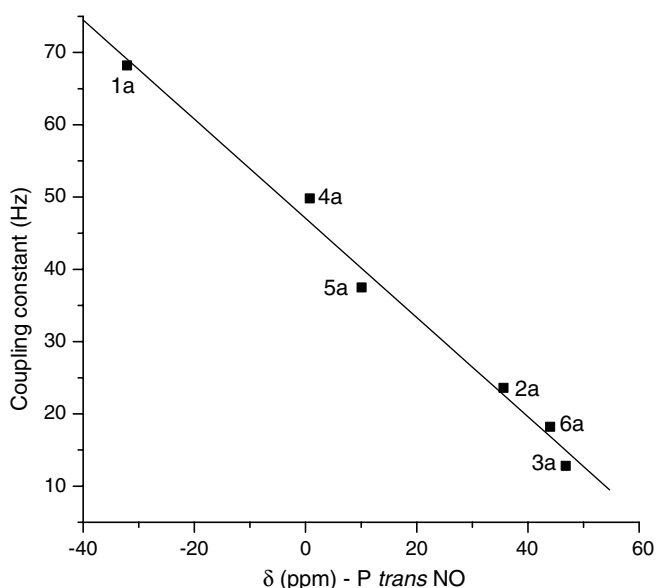


Fig. 10. Correlation between the coupling constants (Hz) and the chemical shifts for the phosphorus *trans* NO in the *mer*- $[\text{RuCl}_3(\text{NO})(\text{P}-\text{P})]$ series ($R = 0.99$).

work, **1a**, **2a**, **3a** and **6a** are stable in solution as demonstrated by ^{31}P $\{^1\text{H}\}$ NMR spectra of solutions followed during a period of a month. Probably, due to steric reasons, the complexes with the larger diphosphines, *dppp* and *dppb*, adopt the *fac* geometry.

3.4. Electrochemistry

The cyclic voltammetric experiments on complexes **1–7** and **1a–6a** were carried out in CH_2Cl_2 and CH_3CN solutions. In CH_2Cl_2 , the CV responses are dominated by irreversible reduction waves, assigned to the reduction of the NO^+ group coordinated to Ru(II) [40,41]. Fig. 11 shows a typical cyclic voltammogram for these complexes and the potentials of the processes are shown in Table 9.

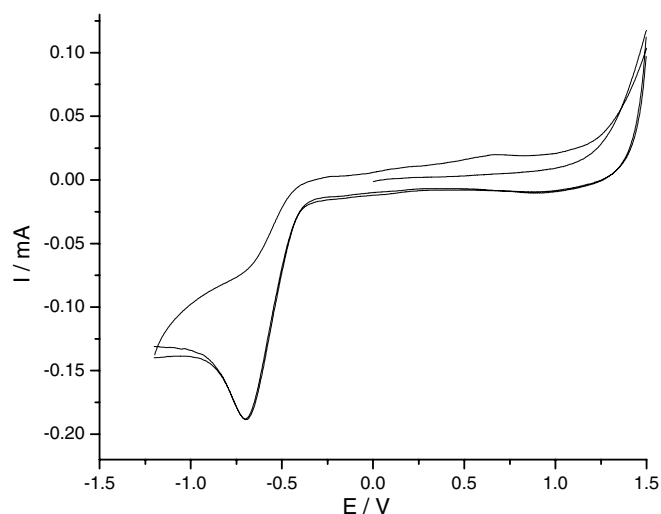


Fig. 11. Cyclic voltammetric response for **2a** in CH_2Cl_2 at 100 mV s^{-1} .

Table 9

Electrochemical data (V) for the series *fac* and *mer* $[\text{RuCl}_3(\text{NO})(\text{P}-\text{P})]$

Complex	CH_2Cl_2		CH_3CN	
	<i>fac</i> - E_{cp}	<i>mer</i> - E_{cp}	<i>fac</i> - $E_{\text{cp}}/E_{\text{ap}}$	<i>mer</i> - $E_{\text{cp}}/E_{\text{ap}}$
1	-0.79	-0.64	-0.50/+1.42	-0.48/+1.89
2	-0.87	-0.70	-0.49/+2.03	-0.52/+1.88
3	-0.73	-0.64	-0.60/+2.06	-0.45/+1.89
4	-0.85	-0.76	-0.60/+2.15	-0.59/+1.81
5	-0.92	-0.80	-0.54/+2.08	-0.45/+1.90
6	-1.00	-1.10	-0.70/+1.80	-0.92/+1.76
7		-0.75		-0.60/+1.77

$E_{\text{cp}} = \text{Ru}^{\text{II}}-\text{NO}^+/\text{Ru}^{\text{II}}-\text{NO}^0$.

$E_{\text{ap}} = \text{Ru}^{\text{II}}-\text{NO}^+/\text{Ru}^{\text{III}}-\text{NO}^+$.

Electrochemical studies of $\text{Ru}-\text{NO}^+$ containing compounds have shown reversible reduction of the NO^+ group at more positive potentials than those observed in this work [40]. For example, previous work from this group [15] has shown that *trans*- $[\text{RuCl}(\text{NO})(\text{dppe})_2]^{2+}$ presents a reversible reduction of the NO^+ ligand at +0.10 V versus

Ag/AgCl. The more negative reduction potentials for the NO^+ , measured for the $[\text{RuCl}_3(\text{NO})(\text{P-P})]$ complexes, result from the replacement of two P atoms (π acceptor/ σ -donor ligand) by two Cl^- (σ -/ π -donor ligand). In this case the ruthenium center becomes electronically richer and consequently, it is more difficult to add an electron to the NO^+ .

The reduction of the coordinated NO^+ group is accompanied by a rapid chemical reaction, hence, there is no sign of a return wave even at low temperature (0°C) and at scan rates of up to 5 V s^{-1} for all compounds studied. In all cases a plot of peak current versus the square root of the scan rate gives a straight line, indicating that the electron-transfer process is diffusion controlled. Application of a switching potential more negative than the NO^+ -based reduction process results in new redox peaks in the cyclic voltammogram, but no additional studies were made to identify such a process.

Utilizing the coordinating solvent CH_3CN in the CV experiments, some other characteristics could be observed (Fig. 12). The irreversible reduction under the NO^+ in this solvent occurred at a considerably less negative potential (ca. 0.30 V) as shown in Table 9. This fact is an additional evidence to confirm that this wave corresponds to the reduction of the NO^+ [40], because electrochemical processes occurring over the ligands are more sensible to changes in the medium.

After the irreversible NO^+ reduction, scanning to positive potential, a new dependent irreversible wave is observed at $+1.0\text{ V}$ for all the compounds. This process can be ascribed to the oxidation of free chlorine present in the solution [11]. Thus, reductions of all compounds are accompanied by loss of chloride. At more positive potentials, an irreversible wave appeared for all complexes

(reversible for **1** and **6a**), a fact that has been attributed to the oxidation of the ruthenium: $\text{Ru}^{\text{II}}\text{-NO}^+/\text{Ru}^{\text{III}}\text{-NO}^+$ [42]. These characteristics can be observed in Fig. 12. The high value for the $\text{Ru}^{\text{II}}/\text{Ru}^{\text{III}}$ potential is explained by the presence of the NO^+ (strong π acceptor) [7]. The dpdm complex shows the lowest potential for these processes, which can be explained by the reduced size of this diphosphine when compared with the others. This fact turns the Ru^{III} oxidation state to be more favorable in this complex than in the others, because the Ru^{III} ion is slightly smaller than Ru^{II} ion [43]. For all the compounds studied, except for **1** and **6a**, the oxidation of Ru^{II} to Ru^{III} is irreversible indicating that the $\text{Ru}^{\text{III}}\text{-NO}^+$ fragments are not stable. After this oxidation, scanning for the cathodic region, another irreversible wave appears. No further investigations were made to characterize this new specie.

The peak potential for the pair $\text{Ru}^{\text{II}}/\text{Ru}^{\text{III}}$ in the $\text{trans-}[\text{RuCl}(\text{NO})(\text{P-P})_2]^{2+}$ complexes was not observed until 2.4 V [15]. For the complex $[\text{RuCl}(\text{NO})(\text{bpy})_2]^{2+}$, the potential for this process was determined in liquid SO_2 as being 3.0 V [44], demonstrating the high electron deficient metal center. Contraparty, this process is observed in the $[\text{RuCl}_3(\text{NO})(\text{P-P})]$ complex showing, in this case, the higher electron density on the metal center because of the presence of two additional chlorides.

Scheme 3 shows the representative equations for the above mentioned electrochemical processes involving the coordinated nitrosyl ligand. In step 1 the compounds are reduced at E_1 , ranging from -640 to -1000 mV , where the site of reduction is the NO^+ group giving the NO^0 radical ligand. The reduced complexes are unstable and a chloride ligand is substituted by a neutral solvent CH_3CN molecule (step 2).

A similar redox induced substitution reaction has been observed in the related compounds $[\text{trans-RuCl}(\text{NO})(\text{cyclam})]^{2+}$ [45] and $[\text{RuCl}_2(\text{dmsO-O})(\text{NO})\text{L}]$, $\text{L} = \text{Cl}^-$ or NO_2^- [11]. The complex $[\text{RuCl}_2(\text{P-P})(\text{NO}^0)(\text{CH}_3\text{CN})]$ is unstable and loses NO^0 , producing the $[\text{RuCl}_2(\text{P-P})(\text{CH}_3\text{CN})_2]$ compound (the processes for these species were not identified).

The electronic density over the NO^+ ligand can be estimated by IR and electrochemical data [46]. There are in the literature some good correlations between these two parameters [47,48]. In this work such correlation between the NO stretching in CH_2Cl_2 solutions and the E_{cp} for the NO^+ reduction in the same solvent was made and is shown in Fig. 13. It is possible to observe a good linearity of the data. The complex with the less energetic ν_{NO} , is that with more electronic density over the NO and consequently the reduction potential in this situation occurred at the more negative value. The complex with the more basic phosphine dcp (p $K_a \approx 10$) [49] is the complex with this characteristics. Following this series, the complex with the more energetic ν_{NO} presents the lower reduction potential for the NO^+ , because the NO , in this case, has less electronic density, and addition of electrons on it is easier (less negative potential).

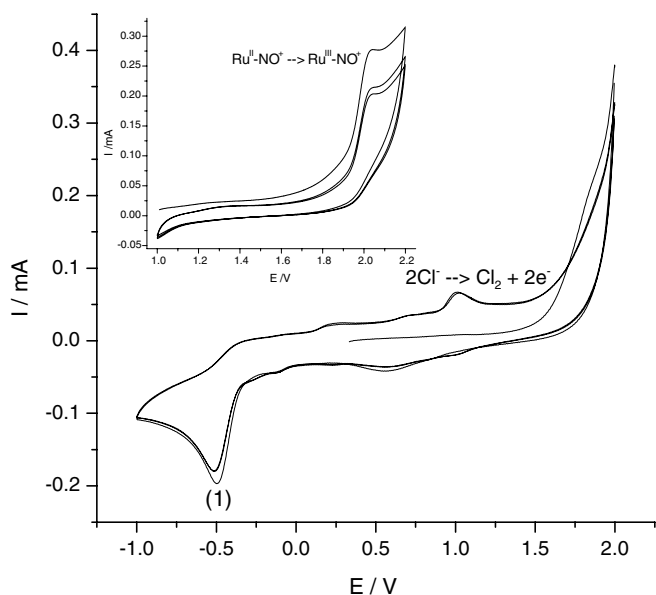
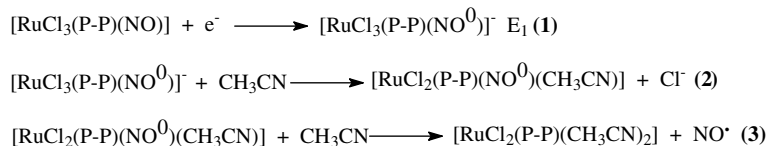
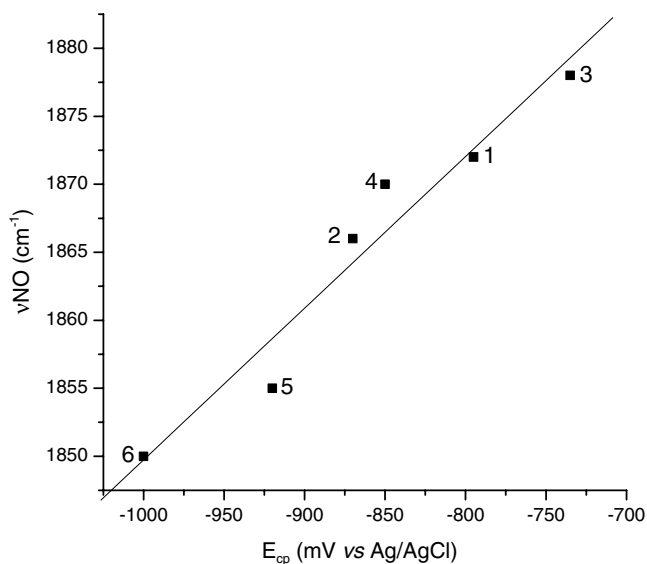


Fig. 12. Cyclic voltammometric response for **2** in CH_3CN at 100 mV s^{-1} . Inset. Same CV in the $1.0\text{--}2.2\text{ V}$ region.

Scheme 3. Electrochemical processes involved in the $[\text{RuCl}_3(\text{P-P})(\text{NO})]$ complexes in CH_3CN .Fig. 13. Correlation between the NO^+ reduction potential and the NO stretching band in CH_2Cl_2 solution for the *fac*- $[\text{RuCl}_3(\text{NO})(\text{P-P})]$ series ($R = 0.97$).

Comparing the series of isomers (*fac* and *mer*) the reduction of the NO^+ in the *mer* ones should be less negative than that observed for the *fac* species because the presence of a phosphorus (π acceptor ligand) *trans* to NO in the *mer* isomers creates a pathway to the distribution of the additional electron density when the NO^+ is reduced to NO^0 , consequently the reduction is more accessible. Analyzing the values from Table 9 it is clear that this expected behavior occurs, mainly with CH_2Cl_2 as solvent. The exception are the compounds **6/6a** in which the *mer* shows a more negative potential, this happens because the *dcppe* diphosphine is much more basic than the other ones, not acting as a good π acceptor.

Considering the oxidation process $\text{Ru}^{\text{II}}/\text{Ru}^{\text{III}}$, in the *mer* isomers such process should occur at lower potential than for the corresponding *fac* compound, because the presence of Cl^- *trans* Cl^- , due to the competitive effect, increases the electron density in the ruthenium center. In fact, this is experimentally observed for all compounds studied with the exception of the *dppm* compounds.

3.5. Structural studies

In all structures of this work the metal displays the expected distorted octahedral coordination geometry where the nitrosyl group is essentially linear, *trans* to Cl^-

in the *fac* **1–4** isomers, *trans* to P in the *mer* **6a** isomers and *trans* to O in **7**. The linearity of this group is consistent with the NO stretching vibration band in the IR spectra, both indicating that the NO group is formally bound to the metal as NO^+ [50,51]. The N–O bond lengths fall in range from 1.029(6) to 1.152(5) Å, being consistent with other reported data [52–54]. In spite of the relatively large differences in the NO distance, such trend is not reflected in the NO stretching frequencies, because for similar values of ν_{NO} , very different N–O distances are found, as seen by comparing the *fac*- $[\text{RuCl}_3(\text{NO})(\text{dppm})]$, $\nu_{\text{NO}} = 1875 \text{ cm}^{-1}$ /N–O = 1.029(6) Å with the *fac*- $[\text{RuCl}_3(\text{NO})(\text{dppp})]$, $\nu_{\text{NO}} = 1875 \text{ cm}^{-1}$ /N–O = 1.152(5) Å.

The equatorial Ru–Cl bond lengths (2.41–2.43 Å) for **1–4** are longer than the axial one (*trans* NO; 2.35–2.37 Å) by ≈ 0.07 Å, consistent with the *trans* strength effect of the NO. In the related complexes *fac*- $[\text{RuCl}_3(\text{NO})(\text{bipy})]$ (*bipy* = 2,2'-bipyridine) [55] and *fac*- $[\text{RuCl}_3(\text{NO})(\text{pdma})]$ (*pdma* = *o*-phenylenebis(dimethyl-arsine)) [56], these differences are 0.03 and 0.07 Å, respectively, indicating that diphosphines and the *pdma* ligand exert a greater *trans* labilizing influence on chloride than does *bipy*.

The Ru–P distances for **1–4** and **7** are in the usual range for Ru–diphosphines complexes varying between 2.35 and 2.38 Å, the same occurring for the Ru–Cl distances that are in the range 2.35–2.45 Å [12–15]. The angles P–Ru–P (bite angle) increase in the order of the chain length of the diphosphines (*dppm* > *c-dppen* > *dpepe* > *dppp*), ranging from 71.26° until 93.22°.

The X-ray structure refinement of **6a** shows a high thermal parameter for the NO group, which results in unusual values for the N–O and Ru–N distances. The Ru–P(1) distance [2.4563(12) Å] is longer than the Ru–P(2) [2.4015(12) Å], because the former is *trans* to the NO^+ , a π acceptor ligand which competes for the same electrons of the metal center with the phosphorus atoms in *trans*. The same is observed for Ru–P(3) and Ru–P(4).

This behavior in the structure of **6a** had been previously observed in the analogous *mer*- $[\text{RuCl}_3(\text{NO})(\text{dppb})]$ [13] and *mer*- $[\text{RuCl}_3(\text{NO})(\text{diop})]$ [14], and in the *cis*- $[\text{Ru}(\text{dpepe})(\text{CO})_2(\text{OSO}_2\text{CF}_3)_2]$ [57]. This last one has a Ru–P distance *trans* to CO longer than the other, *trans* to OSO_2CF_3 , showing the expected similar behavior of the CO when compared with the NO ligand.

In complexes **2** and **7** the formed chelates are of five members, this being the reason for the similarity of the bite angles observed in their X-ray structures, 85.76° and 83.94°, respectively.

The P=O distance of 1.526(5) Å in **7** is approximately the same as observed for *tcc*-[RuCl₂(η²-dppmO)₂] (P=O = 1.50 Å) [58]. The Ru–O distances of 2.059(5) Å in **7** is much shorter than that from the *tcc*-[RuCl₂(η²-dppmO)₂] (2.20 Å), reflecting the presence of the NO⁺ ligand *trans* to the oxygen in the former.

4. Conclusions

We have shown that *mer*-[RuCl₃(NO)(P–P)] isomers can be obtained from the corresponding *fac* isomers in solid state or in solution by using white light. The isomerization processes were followed by IR (in solid state) and ³¹P {¹H} NMR spectra (in CH₂Cl₂ solution). The *mer*-[RuCl₃(¹⁵NO)(dppb)] was used for the attribution of the phosphorus chemical shifts and it was used as a reference for the other similar complexes. The reduction potential for the NO⁺ group is dependent on the solvent used (CH₂Cl₂ or CH₃CN). There is a good correlation between the NO⁺ reduction potential and the NO stretching band in CH₂Cl₂ solution for the *fac*-[RuCl₃(NO)(P–P)] series.

5. Supplementary data

Coordinates and other crystallographic data have been deposited with the CCDC, deposition code 287922–287927, respectively for **3**, **7**, **2**, **1**, **4** and **6a**. Copies of this information may be obtained from The Director, CCDC, 12 Union Road, Cambridge, CB2 1EZ, UK (fax: +44 1233 336033; e-mail: deposit@ccdc.cam.ac.uk or [www:http.ccdc.cam.ac.uk](http://www.ccdc.cam.ac.uk)).

Acknowledgement

We thank CNPq, CAPES, FINEP, PRONEX and FA-PESP for financial support.

References

- [1] D.J. Hodgson, N.C. Payne, J.A. McGinnety, R.G. Pearson, J.A. Ibers, *J. Am. Chem. Soc.* 90 (1968) 4486.
- [2] R.M.J. Palmer, A.G. Ferrige, S. Moncada, *Nature* 327 (1987) 524.
- [3] L.J. Ignarro, G.M. Buga, K.S. Wood, R.E. Byrns, *Circ. Res.* 61 (1987) 866.
- [4] E. Tfouni, M. Krieger, B.R. McGarvey, D.W. Franco, *Coord. Chem. Rev.* 236 (2003) 57.
- [5] R. Bakhtiar, R.E.I. Ochiai, *Gen. Pharmacol.* 32 (1999) 525.
- [6] W.P. Griffith, *The Chemistry of the Rarer Platinum Metals*, Interscience Publishers, New York, 1967.
- [7] D.M.P. Mingos, D.J. Sherman, *Adv. Inorg. Chem.* 34 (1989) 293.
- [8] M.J. Clarke, J.B. Gaul, *Struct. Bond.* 81 (1993) 147.
- [9] P.C. Ford, J. Bourassa, K. Miranda, B. Lee, I. Lorkovic, S. Boggs, S. Kudo, L. Laverman, *Coord. Chem. Rev.* 171 (1998) 185.
- [10] L.G.F. Lopes, A. Wieraszko, Y. El-Sherif, M.J. Clarke, *Inorg. Chim. Acta* 312 (2001) 15.
- [11] B. Serli, E. Zangrando, E. Lengo, G. Mestroni, L. Yellowlees, E. Alessio, *Inorg. Chem.* 41 (2002) 4033.
- [12] A.A. Batista, C. Pereira, S.L. Queiroz, L.A.A. de Oliveira, R.H.A. Santos, M.T.P. Gambardella, *Polyhedron* 16 (1997) 927.
- [13] A.A. Batista, C. Pereira, K. Wohnrath, S.L. Queiroz, R.H.A. Santos, M.T.P. Gambardella, *Polyhedron* 18 (1999) 2079.
- [14] G. Von Poelhsitz, M.P. de Araujo, L.A.A. de Oliveira, S.L. Queiroz, J. Ellena, E.E. Castellano, A.G. Ferreira, A.A. Batista, *Polyhedron* 21 (2002) 2221.
- [15] R.C.L. Zampieri, G. Von Poelhsitz, A.A. Batista, O.R. Nascimento, J. Ellena, E.E. Castellano, *J. Inorg. Biochem.* 92 (2002) 82.
- [16] G. Von Poelhsitz, A.A. Batista, J. Ellena, E.E. Castellano, E.S. Lang, *Inorg. Chem. Commun.* 8 (2005) 805.
- [17] L.R. Dinelli, A.A. Batista, K. Wohnrath, M.P. de Araujo, S.L. Queiroz, M.R. Bonfadini, G. Oliva, O.R. Nascimento, P.W. Cyr, K.S. MacFarlane, B.R. James, *Inorg. Chem.* 38 (1999) 5341.
- [18] Enraf-Nonius, COLLECT, Nonius BV, Delft, The Netherlands, 1997–2000.
- [19] Z. Otwinowski, W. Minor, HKL Denzo Scalepack, in: C.W. Carter Jr., R.M. Sweet (Eds.), *Methods in Enzymology*, vol. 276, Academic Press, New York, 1997, p. 307.
- [20] R.H. Blessing, *Acta Crystallogr.* A51 (1995) 33.
- [21] P. Coppens, in: F.R. Ahmed, S.R. Hall, C.P. Huber (Eds.), *Crystallographic Computing*, Munksgaard, Copenhagen, 1970, p. 255.
- [22] P. Coppens, L. Leiserowitz, D. Rabinovich, *Acta Crystallogr.* 18 (1965) 1035.
- [23] G.M. Sheldrick, SHELXS-97. Program for Crystal Structure Resolution, University of Göttingen, Göttingen, Germany, 1997.
- [24] G.M. Sheldrick, SHELXL-97. Program for Crystal Structures Analysis, University of Göttingen, Göttingen, Germany, 1997.
- [25] L.J. Farrugia, *J. Appl. Crystallogr.* 30 (1997) 565.
- [26] P.C. Ford, S. Weckler, *Coord. Chem. Rev.* 249 (2005) 1382.
- [27] A.K. Patra, P.K. Mascharak, *Inorg. Chem.* 42 (2003) 7363.
- [28] V. Togniolo, R.S. da Silva, A.C. Tedesco, *Inorg. Chim. Acta* 316 (2001) 7.
- [29] J.T. Mague, J.P. Mitchener, *Inorg. Chem.* 11 (1972) 2714.
- [30] C.F. Fortney, S.J. Geib, F.T. Lin, R.E. Shepherd, *Inorg. Chim. Acta* 358 (2005) 2921.
- [31] J.H. Enemark, R.D. Feltham, *Coord. Chem. Rev.* 13 (1974) 339.
- [32] K. Nakamoto, *Infrared and Raman Spectra of Inorganic and Coordination Compounds*, 4th ed., John Wiley & Sons, 1986.
- [33] G.B. Deacon, J.H.S. Green, *Spectrochim. Acta, A-M A* 24 (1968) 845.
- [34] C.A. Tolman, *Chem. Rev.* 77 (1977) 313.
- [35] D.A. Freedman, D.E. Janzen, J.L. Vreeland, H.M. Tully, K.R. Mann, *Inorg. Chem.* 41 (2002) 3820.
- [36] P.G. Douglas, R.D. Feltham, H.G.J. Metzger, *J. Am. Chem. Soc.* 93 (1971) 84.
- [37] P.E. Garrou, *Inorg. Chem.* 14 (1975) 1435.
- [38] L. Carlton, R. Weber, *Inorg. Chem.* 33 (1996) 5843.
- [39] J. Mason, L.F. Larkworthy, E.A. Moore, *Chem. Rev.* 102 (2002) 913.
- [40] R.W. Callahan, T.J. Meyer, *Inorg. Chem.* 16 (1977) 574.
- [41] F. Baumann, W. Kaim, L.M. Baraldo, L.D. Slep, J.A. Olabe, J. Fiedler, *Inorg. Chim. Acta* 285 (1999) 129.
- [42] D. Ooyama, N. Nagao, H. Nagao, Y. Sugimoto, F.S. Howell, M. Mukaida, *Inorg. Chim. Acta* 261 (1997) 45.
- [43] D.D. Walker, H. Taube, *Inorg. Chem.* 20 (1981) 2828.
- [44] D.W. Pipes, T.J. Meyer, *Inorg. Chem.* 23 (1984) 2466.
- [45] D.R. Lang, J.A. Davis, L.G.F. Lopes, A.A. Ferro, L.C.G. Vasconcellos, D.W. Franco, E. Tfouni, A. Wieraszko, M.J. Clarke, *Inorg. Chem.* 39 (2000) 2294.
- [46] J.A. McCleverty, *Chem. Rev.* 79 (1979) 53.
- [47] M.G. Sawaia, R.S. da Silva, *Transition Metal Chem.* 28 (2003) 254.
- [48] L.G.F. Lopes, M.G. Gomes, S.S.S. Borges, D.W. Franco, *Aust. J. Chem.* 51 (1998) 865.

- [49] M. Rahman, H. Liu, K. Eriks, A. Prock, W. Giering, *Organometallics* 8 (1989) 1.
- [50] G.B. Richter-Addo, P. Legzdins, *Metal Nitrosyls*, Oxford University Press, New York, 1992.
- [51] H. Tomizawa, K. Harada, E. Miki, K. Mizumachi, T. Ishimori, A. Urushiyama, A.M. Nakahara, *Bull. Chem. Soc. Jpn.* 66 (1993) 1658.
- [52] R. Eisenberg, C.D. Meyer, *Acc. Chem. Res.* 8 (1975) 26.
- [53] K.R. Coll, J.E. Fergusson, V. McKee, C.T. Page, W.T. Robinson, T.S. Keong, *Inorg. Chem.* 26 (1987) 106.
- [54] H. Hadadzadeh, M.C. DeRosa, G.P.A. Yap, A.R. Rezvani, R.J. Crutchley, *Inorg. Chem.* 41 (2002) 6521.
- [55] M. Haukka, T. Venäläinen, M. Ahlgrén, T.A. Pakkanen, *Inorg. Chem.* 34 (1995) 2931.
- [56] B.J. Coe, C.I. McDonald, R.L. Beddoes, *Polyhedron* 17 (1998) 1997.
- [57] M.F. Mahon, M.K. Whittlesey, P.T. Wood, *Organometallics* 18 (1999) 4068.
- [58] M.P. Felicissimo, A.A. Batista, A.G. Ferreira, J. Ellena, E.E. Castellano, *Polyhedron* 24 (2005) 1063.